

Interactions of the $3p\pi_u c^1\Pi_u(v=2)$ Rydberg-complex member in isotopic N_2

M. O. Vieitez,¹ T. I. Ivanov,¹ C. A. de Lange,¹ W. Ubachs,^{1,a)} A. N. Heays,² B. R. Lewis,² and G. Stark³

¹*Department of Physics and Astronomy, Laser Centre, Vrije Universiteit, De Boelelaan 1081, 1081 HV Amsterdam, The Netherlands*

²*Research School of Physical Sciences and Engineering, The Australian National University, Canberra, ACT 0200, Australia*

³*Department of Physics, Wellesley College, Wellesley, Massachusetts 02481, USA*

(Received 3 January 2008; accepted 28 January 2008; published online 7 April 2008)

The $3p\pi_u c^1\Pi_u-X^1\Sigma_g^+(2,0)$ Rydberg and $b'^1\Sigma_u^+-X^1\Sigma_g^+(7,0)$ valence transitions of $^{14}N_2$, $^{14}N^{15}N$, and $^{15}N_2$ are studied using laser-based 1 extreme ultraviolet (XUV)+1' UV two-photon-ionization spectroscopy, supplemented by synchrotron-based photoabsorption measurements in the case of $^{14}N_2$. For each isotopomer, effective rotational interactions between the $c(v=2)$ and $b'(v=7)$ levels are found to cause strong Λ -doubling in $c(v=2)$ and dramatic P/R -branch intensity anomalies in the $b'-X(7,0)$ band due to the effects of quantum interference. Local perturbations in energy and predissociation line width for the $c(v=2)$ Rydberg level are observed and attributed to a spin-orbit interaction with the crossing, short-lived $C^3\Pi_u(v=17)$ valence level. © 2008 American Institute of Physics. [DOI: 10.1063/1.2883955]

I. INTRODUCTION

The level structure of the nitrogen molecule in the region of its dipole-allowed absorption spectrum (i.e., above $100\,000\text{ cm}^{-1}$) is one of severe complexity. First, the singlet states that can be accessed directly in the extreme ultraviolet (XUV) region via allowed transitions behave seemingly erratically. Numerous investigations have been performed to unravel these singlet structures. Through the semiempirical work of Stahel *et al.*,¹ the lowest-energy dipole-allowed spectrum of N_2 has been explained by considering the homogeneous electrostatic interactions between the Rydberg and valence states of $^1\Sigma_u^+$ and $^1\Pi_u$ symmetries. In particular, the corresponding calculated vibronic band strengths¹ showed strong quantum-interference effects. Later, a quantitatively improved model of the N_2 spectrum, based on *ab initio* calculations, was put forward by Spelsberg and Meyer.² Edwards *et al.*³ extended the description by incorporating heterogeneous, rotationally dependent interactions in the coupling model. Nevertheless, there remain many details in the structure of the singlet states to be discovered and explained. The theoretical and experimental study of rotationally dependent perturbations in the Rydberg-valence singlet manifold of N_2 and its isotopomers ($^{15}N_2$ and $^{14}N^{15}N$) has been a topic of recent interest. Strong local perturbations can give rise, not only to level shifts, but also to changes in intensities. By analogy with the vibronic case, such perturbations can cause rotational quantum-interference effects, leading, in some cases, to complete damping of intensity.⁴

Second, the singlet states show predissociation behavior that is also erratic. Four decades ago, Carroll and Collins⁵ noted that, of the vibrational levels of the $b^1\Pi_u$ valence

state, only $v=1, 5$, and 6 could be observed in emission. The predissociation rates pertaining to the $b^1\Pi_u(v)$ levels have been determined experimentally from line-width studies employing either synchrotron-radiation⁶ or narrow-bandwidth XUV laser-radiation^{7,8} sources. The XUV laser technique is especially suitable for the determination of excited-state lifetimes with rotational resolution. In addition, complementary pump-probe experiments employing picosecond lasers have been carried out to determine lifetimes experimentally.⁹ Numerous additional investigations have been performed in order to produce a quantitative experimental database for the predissociation rates of the singlet states of N_2 , including translational-spectroscopic studies,^{10,11} and investigations focusing specifically on the $^{15}N_2$ and $^{14}N^{15}N$ isotopomers.¹² Knowledge of the N_2 predissociation behavior and mechanism is a prerequisite for a detailed understanding of radiative-transfer processes, as well as stratospheric chemistry, in nitrogen-rich planetary atmospheres such as those of the Earth and Titan.

Over the years, a large effort has been invested towards an understanding of the origin of the predissociation in the lowest-lying electric-dipole-accessible singlet states of N_2 .¹³ Since the singlet states couple via homogeneous spin-orbit interaction to the $C^3\Pi_u$ state, which, in turn, is coupled to the $C'^3\Pi_u$ state above its dissociation limit, a detailed understanding of the predissociation of the singlet states requires consideration of the interactions within the triplet manifold. A recent study by Lewis *et al.*,¹⁴ based on a coupled-channel Schrödinger equation (CSE) model for the interacting $^1\Pi_u(b, c, o)$ and $^3\Pi_u(C, C')$ states, has provided a quantitative explanation for the predissociation mechanism of the $^1\Pi_u$ states in the energy region below $105\,000\text{ cm}^{-1}$. This model achieves spectroscopic accuracy and builds upon the information gathered over the years concerning low-lying

^{a)}Electronic mail: wimu@nat.vu.nl.

vibrational levels of the $C^3\Pi_u$ and $C'^3\Pi_u$ states, starting with the benchmark study by Carroll and Mulliken.¹⁵ These triplet data are reviewed in Ref. 14. Additional information beyond $C^3\Pi_u(v=5)$ and $C'^3\Pi_u(v=2)$ has been obtained indirectly by examining the predissociative effect of these states on the singlet manifold, guided by *ab initio* potential curves and an extrapolation from the known lower levels. The CSE model is capable of explaining the predissociation rates for $b^1\Pi_u(v\leq 6)$, with rotational resolution, for the three isotopomers $^{15}\text{N}_2$, $^{14}\text{N}^{15}\text{N}$, and $^{14}\text{N}_2$.¹⁶ In particular, the $b^1\Pi_u(v=1)$ level of $^{14}\text{N}_2$ provides a good test for the model. For low J , the predissociation rate is very small and decay is mainly radiative, with an exceptionally long lifetime.¹⁷ The predicted predissociation rate increases steeply with J , in good agreement with experiment.¹⁸

In order to extend our understanding of the predissociation phenomenon in N_2 into the excitation region above $105\,000\text{ cm}^{-1}$, significant CSE-model development is necessary, facilitated by new experimental measurements. In particular, this requires knowledge of the locations of higher vibrational levels of the $C^3\Pi_u$ valence state, together with a consideration of the other triplet Rydberg states, $F^3\Pi_u$,¹⁹ and $G^3\Pi_u$,²⁰ that play the role of inducing further predissociation through their interactions with the $C^3\Pi_u$ and $C'^3\Pi_u$ states and direct spin-orbit coupling to the $^1\Pi_u$ states.²¹

Electric-dipole transitions from the $X^1\Sigma_g^+$ ground state of N_2 to the triplet manifold are spin-forbidden, thus limiting the information that can be obtained directly on these states using normal spectroscopic techniques. However, spin-orbit interactions cause coupling between the singlet and triplet manifolds, leading to local perturbations in the singlet states that can be observed using narrow-bandwidth spectroscopic techniques, providing useful information on the triplet states indirectly. For example, the $C^3\Pi_u(v)$ valence-state levels, which have low rotational constants, are most likely to cross, and interact with, levels of the Rydberg states of N_2 , which have significantly higher rotational constants. Indeed, spectroscopic parameters for the $C^3\Pi_u(v=14)$ level of $^{15}\text{N}_2$ have been reported recently, determined by analyzing its perturbation of $c^1\Pi_u(v=1)$ near $106\,500\text{ cm}^{-1}$, including the observation of a few extra lines due to transitions to the perturbing level.^{22,23}

The $3p\pi_u c^1\Pi_u$ state is a member of the $3p$ Rydberg complex of N_2 ,²⁴ which also includes the $3p\pi_u G^3\Pi_u$, $3p\sigma_u c^1\Sigma_u^+$, and $3p\sigma_u D^3\Sigma_u^+$ states. The c and G states exhibit a (small) spin-orbit interaction, while the G and D states, and the c and c' states, exhibit strong rotational interactions which perturb the rotational constants and contribute to Λ -doubling in the Π_u $3p$ -complex components, leading to a good deal of spectral complexity. In the present study, we investigate the spectroscopy and predissociation characteristics of the $c^1\Pi_u(v=2)$ $3p$ -complex member in the energetic region of $108\,500$ – $109\,500\text{ cm}^{-1}$, for all three N_2 isotopomers, using principally $1\text{XUV}+1'\text{UV}$ two-photon-ionization spectroscopy. This level is perturbed by singlet valence states occurring in this energy region, most notably $b^1\Pi_u(v=11)$ and $b'^1\Sigma_u(v=7)$, the latter of which contributes to observable Λ -doubling effects and quantum-interference phenomena. Local perturbations in the $c^1\Pi_u(v$

$=2$) level, caused by these singlet levels, as well as those due to $C^3\Pi_u(v=17)$, are studied, together with associated predissociative effects.

II. EXPERIMENTAL METHODS

A. XUV laser spectroscopy

Laser-based $1\text{XUV}+1'\text{UV}$ two-photon-ionization spectroscopy is the primary technique employed here to study the excitation spectrum of N_2 , in the range $\lambda=91.3$ – 92.3 nm . Details of the experimental method, including a description of the lasers, vacuum setup, molecular-beam configuration, time-of-flight (TOF) detection scheme, and calibration procedures, have been presented previously.²⁵ Briefly, narrow-bandwidth XUV radiation is produced by frequency tripling the UV light from a frequency-doubled pulsed dye laser (PDL) pumped by an injection-seeded Nd: yttrium aluminum garnet (YAG) laser. Frequency tripling takes place in a free Xe-jet expansion, where the UV power (25 mJ in 5 ns) is focused. The frequency in the XUV range is calibrated against a Doppler-broadened I_2 linear-absorption spectrum,²⁶ recorded simultaneously using part of the visible output of the dye laser. An absolute accuracy of $\sim 0.1\text{ cm}^{-1}$ for fully resolved line positions is estimated.

A skimmed, pulsed N_2 beam is perpendicularly intersected by temporally and spatially overlapping XUV and UV laser beams. Nitrogen molecules are excited resonantly by the XUV photons and subsequently ionized by the intense UV light. N_2^+ ions are detected using a TOF mass selector. In addition to normal N_2 , isotopically enriched samples of $^{14}\text{N}^{15}\text{N}$ and $^{15}\text{N}_2$ are also studied. The TOF technique employed allows for mass identification of the N_2^+ ions, which can thus be distinguished from ions arising from the background oil in the vacuum system.

The experimental parameters were established to provide the highest N_2 rotational temperature in the interaction region. This was achieved by increasing the N_2 density ($\sim 2 \times 10^{-5}\text{ mbar}$) and therefore increasing the population of the higher rotational levels through collisions between the molecular beam and the higher-pressure background N_2 . To achieve the background pressure required, the nozzle-skimmer distance was kept to a minimum. We thereby recorded spectra associated with two distinct rotational temperatures, one belonging to the supersonic expansion of the molecular beam ($\sim 10\text{ K}$) and one belonging to the background gas at ambient temperature ($\sim 300\text{ K}$). Moreover, by changing the relative delay between the N_2 pulsed-valve trigger and the laser pulse, the rotational temperature in the molecular beam could be selected to measure independent spectra of “cold” (10–50 K) and “warm” (200–300 K) samples. These options helped greatly in the assignment of the spectral lines.

The instrumental contribution to the measured line widths depends on the ambient gas pressure, the settings for measuring cold or warm spectra, the wavelength range, the dye used, and the alignment of the PDL.²⁵ In the case of the high-temperature spectra, an additional Doppler broadening amounting to $\sim 0.25\text{ cm}^{-1}$ full-width at half-maximum (FWHM) must be accounted for in the line-width analyses.

The instrumental width is determined from observed transitions in the $c' \ ^1\Sigma_u^+ - X \ ^1\Sigma_g^+(2,0)$ band, because of its close proximity to the $c \ ^1\Pi_u - X \ ^1\Sigma_g^+(2,0)$ transitions that are measured under virtually the same experimental conditions. The $c'(v=2)$ level is known to be slightly predissociated,⁹ but not to the extent that it will induce significant line broadening in the present experiments. Hence, the instrumental width can be taken to equal the observed width for these transitions. The values obtained for the instrumental contribution to the line width are $0.34 \pm 0.04 \text{ cm}^{-1}$ FWHM for $^{15}N_2$, $0.42 \pm 0.04 \text{ cm}^{-1}$ FWHM for $^{14}N^{15}N$, and $0.40 \pm 0.02 \text{ cm}^{-1}$ FWHM for $^{14}N_2$. Note that the instrumental width also includes the Doppler contribution. The differences between these values are not so much related to the isotopomers, but rather to the specific experimental conditions employed.

Using this narrow-bandwidth XUV laser system, line positions, line widths, and relative intensity variations can be measured with rotational resolution. Information on the predissociation process can be obtained through several complementary means. The lifetime τ (s) of the excited level, shortened due to predissociation, can be expressed as

$$\tau = \frac{1}{2\pi c\Gamma}, \quad (1)$$

where Γ is the natural (Lorentzian) line width (in cm^{-1} FWHM). Under our experimental conditions, Doppler broadening is also present, contributing to the effective instrumental profile which can be taken to be Gaussian.²⁷ Thus, the measured line shape has a Voigt profile, with a width of $\Delta\nu_{\text{obs}}$ FWHM. The Lorentzian line-width component, principally due to predissociation, can be obtained by deconvolution of the experimental Voigt profile using the appropriate Gaussian instrumental profile, of width $\Delta\nu_{\text{inst}}$ FWHM. With some approximations,²⁸ the following relation is obtained:

$$\Gamma = \Delta\nu_{\text{obs}} - \frac{(\Delta\nu_{\text{inst}})^2}{\Delta\nu_{\text{obs}}}. \quad (2)$$

Hence, using Eqs. (1) and (2), the excited-state lifetime τ can be derived straightforwardly from the line-width measurements. In addition, the shortening of the lifetime due to predissociation will not only cause line broadening, but also a decrease in signal intensity, since the detected ions result from the ionization of a decaying excited level. The resulting ionization signal is proportional to the lifetime of the excited intermediate state that is ionized.²⁷ Thus, the intensity depletion also provides information on the predissociation behavior of the excited state, in fact, more sensitively, in many cases, than from direct line-width measurements.

B. XUV synchrotron spectroscopy

Relative ionization signals in the spectra obtained using the two-photon-ionization spectroscopic technique described in Sec. II A are influenced, not only by the aforementioned competition between predissociation and ionization, but also by the inherent oscillator strengths of the transitions. Thus, successful interpretation of the ionization spectra will, in some cases, require a detailed knowledge of the oscillator strengths, the measurement of which requires a different ex-

perimental technique. Therefore, in the case of the $b' - X(7,0)$ transition of $^{14}N_2$, the present ionization spectra are interpreted using oscillator strengths derived from absolute XUV photoabsorption spectra obtained at the 2.5 GeV storage ring of the Photon Factory, a synchrotron radiation facility at the High Energy Accelerator Research Organization in Tsukuba, Japan. These measurements form part of the extensive experimental campaign of Stark *et al.*,^{6,29} who have described the apparatus in detail. Briefly, a 6.65 m spectrometer with a 1200 grooves/mm grating (blazed at 550 nm and used in the sixth order) provides an instrumental resolving power of $\sim 150\,000$, equivalent to a resolution of $\sim 0.7 \text{ cm}^{-1}$ FWHM. The spectrometer tank, filled with N_2 of normal isotopic composition in a flowing configuration, serves as an absorption cell with a path length of ~ 12.5 m and a temperature of 295 K. Rotational-line oscillator strengths and Lorentzian predissociation line-width components are obtained from the experimental photoabsorption cross sections using a nonlinear least-squares fitting procedure which takes account of the finite instrumental resolving power. The line oscillator strengths are converted into equivalent absolute band oscillator strengths using appropriate Hönl-London and Boltzmann factors. Predissociation linewidths determined from these synchrotron-based spectra for the $c(v=2)$ level of $^{14}N_2$ are also used in Sec. IV C to supplement the present laser-based results which, for this isotopomer, do not extend to high-enough J values to access the principal region of interest, i.e., the crossing region with $C(v=17)$.

III. CSE CALCULATIONS

Due to the many interactions associated with levels of the $3p$ Rydberg complex, the interpretation of the corresponding spectra is difficult without some recourse to the theoretical aspects. Therefore, although the present work is, in principle, an experimental study, some CSE calculations have been performed in order to supplement the analysis.

The CSE model employed in this work, an extension of the $(^1\Pi_u + ^3\Pi_u)$ Rydberg-valence model of Lewis *et al.*¹⁴ and Haverd *et al.*,¹⁶ which includes $^1\Sigma_u^+$ Rydberg and valence states and their mutual electrostatic interactions, together with $^1\Sigma_u^+ \sim ^1\Pi_u$ rotational interactions, is described and applied in Liu *et al.*³⁰ and Liang *et al.*³¹ Briefly, the coupled-channel Schrödinger equation is solved for the radial wave functions of a series of interacting diabatic electronic molecular states defined by potential-energy curves and off-diagonal coupling parameters, and the corresponding photo-dissociation cross section from the ground state is computed, yielding line positions and oscillator strengths. The formalism of the technique is described, e.g., by van Dishoeck *et al.*³² and Lewis *et al.*³³ A major advantage of this method is that, after optimization to the well-known singlet energy levels of the $^{14}N_2$ isotopomer, reliable interpolations and extrapolations may be made to previously unknown $^{15}N_2$ and $^{14}N^{15}N$ levels. Additionally, because unbound states are included among the coupled channels, predissociation line widths can be modeled, and so observed line-width pertur-

TABLE I. Observed transition energies (in cm^{-1}) for the $c\ ^1\Pi_u - X\ ^1\Sigma_g^+(2,0)$ band in $^{15}\text{N}_2$. Wave numbers derived from blended lines are flagged with an asterisk (*). Transitions that have not been included in the singlet-singlet deperturbation analysis are marked with a cross-hatch (#).

J''	$R(J'')$	$Q(J'')$	$P(J'')$
0	108 558.19		
1	108 561.52*	108 554.46	
2	108 564.14	108 553.81	108 547.07
3	108 566.65	108 552.83	108 542.77
4	108 569.19*	108 551.62	108 538.09
5	108 570.61#	108 549.99*	108 533.09*
6		108 548.10#	108 527.97#
7	108 573.58*	108 545.88#	108 522.37#
8	108 574.19*		
9		108 540.72#	108 510.34#
10	108 574.19*	108 537.13#	108 503.29*
11	108 573.58*	108 533.09*	108 496.29#
12	108 571.64#	108 530.30#	108 488.13#
13	108 569.18*	108 524.79#	108 481.02#
14	108 565.94	108 519.35*	108 471.40#
15	108 561.78	108 513.33	108 461.49
16	108 556.52	108 506.54	108 450.91
17	108 549.93*	108 498.81	108 439.30
18	108 541.75	108 489.72#	108 426.73
19	108 531.61#	108 478.67#	108 412.76
20	108 519.35*	108 465.30#	
21	108 503.29*	108 448.68#	
22	108 483.94#	108 428.08#	108 359.65#
23		108 403.45#	
24		108 374.59#	
25		108 336.58#	

bations of singlet states may enable the indirect determination of potential-energy curves for the triplet manifold as well as singlet-triplet coupling parameters.

The role of the present CSE modeling is to act as an intelligent extrapolator to support the positive identification of $C(v=17)$ as the perturber of $c(v=2)$. A comparison of experimental versus CSE-model band origins and rotational constants for the $C\ ^3\Pi_u(v \leq 9)$ levels is given in Lewis *et al.*,¹⁴ showing excellent agreement. Further confidence in the rather large extrapolation to $v=17$ is found in the physically based *ab initio* $C\ ^3\Pi_u$ potential-energy curve used within the model, as well as indirect verification of intermediate $C(v)$ levels through the perturbative effects they produce on allowed singlet transitions.²³

IV. RESULTS AND DISCUSSION

A. The $c\ ^1\Pi_u(v=2)$ and $b'\ ^1\Sigma_u^+(v=7)$ levels

Rotationally resolved spectra of the $c\ ^1\Pi_u - X\ ^1\Sigma_g^+(2,0)$ and $b'\ ^1\Sigma_u^+ - X\ ^1\Sigma_g^+(7,0)$ bands in $^{15}\text{N}_2$, $^{14}\text{N}^{15}\text{N}$, and $^{14}\text{N}_2$ were recorded, for a range of rotational temperatures. The corresponding transition energies and line assignments deduced from the spectra are presented in Tables I–VI.

A high-temperature spectrum of the $c\ ^1\Pi_u - X\ ^1\Sigma_g^+(2,0)$ band in $^{15}\text{N}_2$ is shown in Fig. 1, where, with the aid of the diamond-shaped symbols, it can be seen that there is a spectacular deviation from a Boltzmann distribution in the Q -branch rotational intensities. This effect, present in all

TABLE II. Observed transition energies (in cm^{-1}) for the $b'\ ^1\Sigma_u^+ - X\ ^1\Sigma_g^+(7,0)$ band in $^{15}\text{N}_2$. For explanation of the annotations, see caption to Table I.

J''	$R(J'')$	$P(J'')$
0	108 804.36*	
1	108 805.48*	
2	108 805.48*	108 792.74
3	108 804.36*	108 786.78
4	108 802.03	108 779.44
5	108 798.42	108 770.84
6	108 793.90	108 761.09
7	108 788.14	108 750.07
8	108 781.29	
9	108 773.37	
10	108 764.46	
11	108 754.48	
12	108 743.34	
13	108 731.13	108 661.67
14	108 717.70	
15	108 702.66	108 623.54
16		108 602.64
17		108 580.25

branches, made the line assignments somewhat difficult. Finally, these were established by using combination differences for the P - and R -branches, the 3:1 ratio between odd- and even- J'' lines associated with $^{15}\text{N}_2$ nuclear-spin statistics, and the cold and warm spectral recordings. From Fig. 1, it

TABLE III. Observed transition energies (in cm^{-1}) for the $c\ ^1\Pi_u - X\ ^1\Sigma_g^+(2,0)$ band in $^{14}\text{N}^{15}\text{N}$. For explanation of the annotations, see caption to Table I.

J''	$R(J'')$	$Q(J'')$	$P(J'')$
0	108 628.39*		
1	108 631.61	108 624.43	
2	108 634.53	108 623.72	108 616.82
3	108 637.04*	108 622.81*	108 012.77*
4	108 639.39*	108 621.52	108 607.62
5	108 641.37	108 619.89	108 602.54*
6	108 642.83*	108 617.94	108 597.11
7	108 643.76*	108 615.57*	108 591.29
8	108 644.64*	108 612.77*	108 585.15
9	108 644.64*	108 609.76	108 578.56
10	108 644.64*	108 606.42*	108 571.67
11	108 643.76*	108 602.54*	108 564.14
12	108 642.83*	108 598.23	108 556.05
13	108 639.39*	108 593.62	108 547.59
14	108 637.04*	108 588.44	108 538.33
15	108 632.75	108 582.63*	108 528.65
16	108 628.39*	108 576.32	108 517.77
17	108 622.81*	108 569.16#	108 506.18
18	108 615.57#	108 561.40#	108 493.40#
19	108 606.42#	108 551.90#	108 480.93#
20	108 595.48#	108 540.56#	
21	108 582.63#	108 526.83#	
22	108 566.99#	108 509.86#	
23		108 489.18#	
24	108 524.41#		
25	108 504.47#		

TABLE IV. Observed transition energies (in cm^{-1}) for the $b'^1\Sigma_u^+ - X^1\Sigma_g^+(7,0)$ band in $^{14}\text{N}^{15}\text{N}$. For explanation of the annotations, see caption to Table I.

J''	$R(J'')$	$P(J'')$
0	108 880.90*	
1	108 882.06*	108 874.20
2	108 882.06*	108 869.13
3	108 880.90*	108 862.74
4	108 878.69	108 855.17
5	108 875.29*	108 846.41
6	108 870.74	108 836.40
7	108 864.94	108 825.39
8	108 858.15	108 812.91
9	108 850.34	108 799.44
10	108 841.55	
11	108 831.80	108 769.05
12	108 821.08	108 753.21
13	108 809.49	
14	108 797.10	
15	108 783.71	108 698.09
16		108 678.06
17		108 656.94

can be seen that there is a significant intensity decrease between $Q(6)$ and $Q(13)$, with the $Q(8)$ line too weak to be observed. Transitions terminating on levels between $J=5$ and $J=13$ also show a marked intensity decrease in the P - and R -branches. As will be seen below, this intensity depletion is attributed to the effects of the crossing of $c(v=2)$ by the predissociated $v=17$ level of the triplet state $C^3\Pi_u$. In the case of $^{14}\text{N}^{15}\text{N}$, small intensity deviations are observed for transitions to both e - and f -parity levels of $c(v=2)$ with $J=17$ and 18. No unusual intensity behavior is observed in the case of $^{14}\text{N}_2$, where $J=19$ is the highest rotational level of the excited state probed experimentally.

TABLE V. Observed transition energies (in cm^{-1}) for the $c^1\Pi_u - X^1\Sigma_g^+(2,0)$ band in $^{14}\text{N}_2$. For explanation of the annotations, see caption to Table I.

J''	$R(J'')$	$Q(J'')$	$P(J'')$
0	108 698.17*		
1	108 701.57	108 694.06	
2	108 704.51	108 693.35	108 686.60
3	108 707.06*	108 692.27	108 681.91*
4	108 709.54*	108 690.87	108 676.68
5	108 711.55	108 689.15	108 671.31*
6	108 713.09	108 687.04	108 665.79
7	108 714.16*	108 684.68	108 659.69
8	108 714.69*	108 681.91*	108 653.30
9	108 714.69*	108 678.71	108 646.52
10	108 714.69*	108 675.12	108 639.14
11	108 714.16*	108 671.31*	108 631.45
12	108 712.03	108 666.88	108 623.10
13	108 709.54*	108 662.02	108 614.28
14	108 707.06*	108 656.84	108 604.74
15	108 702.84	108 651.00	108 594.55
16	108 698.17*	108 644.69	108 583.56
17		108 637.56	108 571.84
18		108 629.70 _#	108 559.03
19		108 620.80 _#	

TABLE VI. Observed transition energies (in cm^{-1}) for the $b'^1\Sigma_u^+ - X^1\Sigma_g^+(7,0)$ band in $^{14}\text{N}_2$. For explanation of the annotations, see caption to Table I. The information derived from shoulders in the spectra is marked with an s.

J''	$R(J'')$	$P(J'')$
0	108 954.80	
1	108 956.40*	108 948.19
2	108 956.40*	108 942.84
3	108 955.38	108 936.35
4	108 953.17	108 928.52
5	108 949.72	108 919.67
6	108 945.00	108 909.34
7	108 939.26	108 897.80
8	108 932.43	108 885.20
9	108 924.61	108 871.63s
10	108 915.91	108 856.94
11	108 906.24	
12	108 895.50	
13	108 884.08	
14	108 872.15s	
15	108 859.21	
16	108 845.84	

The overall singlet structure in the region of the $v=2$ level of the $3p$ Rydberg complex of N_2 is summarized in Fig. 2 for the e -parity levels of each isotopomer. The plotted points represent a combination of measurements taken using the present apparatus and data from the Harvard-Smithsonian molecular database.³⁴ This structure is completely analogous to that reported and discussed in detail by Sprengers *et al.*¹² for the $v=1$ level of the same Rydberg complex in $^{15}\text{N}_2$, where the interacting valence states are $b(v=8)$ and $b'(v=4)$. In the present case, the diabatic $c^1\Pi_u(v=2)$ and the lower-lying $c'^1\Sigma_u^+(v=2)$ levels exhibit the first-order heterogeneous L -uncoupling interaction characteristic of p -complex members,²⁴ providing the root cause of the J -dependent Λ -doubling in $c(v=2)$. In addition, the higher-lying valence levels, $b^1\Pi_u(v=11)$ and $b'^1\Sigma_u^+(v=7)$, with lower rotational constants, interact homogeneously with the

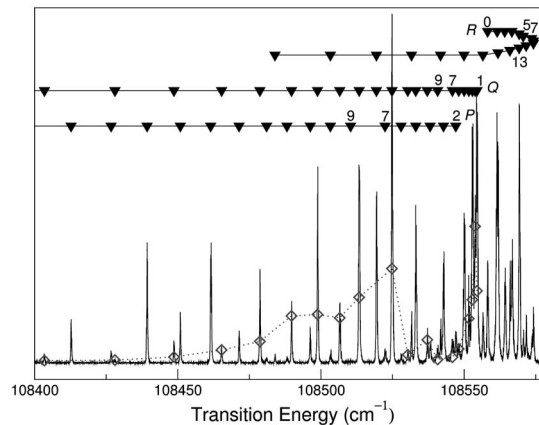


FIG. 1. 1 XUV+1' UV ionization spectrum and line assignments for the $c^1\Pi_u - X^1\Sigma_g^+(2,0)$ band of $^{15}\text{N}_2$. The diamond-shaped symbols act as a guide to indicate the perturbed intensity pattern in the Q branch, where the 3:1 ratio between odd- and even- J'' transition lines, arising from nuclear-spin statistics, has been taken into account.

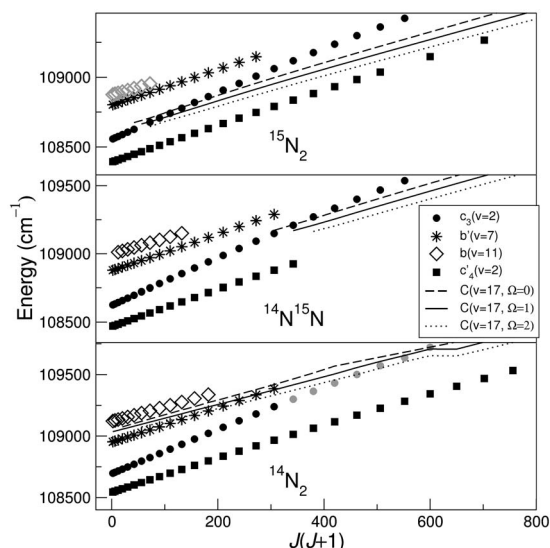


FIG. 2. Rotational term values for $b^1\Pi_u(v=11)$, $b'^1\Sigma_u^+(v=7)$, $c^1\Pi_u(v=2)$, and $c'^1\Sigma_u^+(v=2)$ for the three isotopomers of N_2 . For clarity, only the e -parity levels are displayed. The symbols in gray represent data from the Harvard-Smithsonian molecular database (Ref. 34). Indicative $C^3\Pi_u(v=17)$ energy levels (lines) were obtained using the CSE model. The missing rotational levels for $C(v=17)$ were difficult to determine due to excessive predissociation and additional perturbation by the $F^3\Pi_u(v=2)$ level.

$c^1\Pi_u(v=2)$ and $c'^1\Sigma_u^+(v=2)$ Rydberg levels, respectively, more strongly as J increases. In the case of the f -parity levels, $c^1\Pi_u(v=2) \sim b^1\Pi_u(v=11)$ is the only operative interaction. In reality, in the case of the e levels, the four singlet states form a Rydberg-valence complex, with mutual *effective* interactions arising from the basis couplings just detailed. For example, $b'(v=7)$ and $c(v=2)$, the principal levels studied here, exhibit an effective rotational interaction which culminates in an avoided crossing at intermediate J values, providing a further dimension to the J -dependence of the $c(v=2)$ Λ -doubling. The observed Λ -doublings for the $c(v=2)$ levels of the three isotopomers (shown in Fig. 3) are seen to exhibit qualitatively similar behavior. In the case of $^{15}N_2$, the Λ -doubling is very similar to that reported for the $c(v=1)$ p -complex member of the same isotopomer by Sprengers *et al.*¹² At low J , the effective $c'(v=2)$ contribution to the Λ -doubling is a little more important, with the e

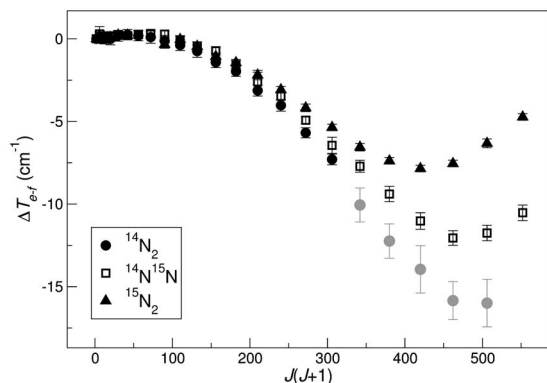


FIG. 3. Observed Λ -doubling [$\Delta T_{e-f} = T_e(J) - T_f(J)$] for the $c^1\Pi_u(v=2)$ Rydberg levels of isotopic N_2 . The symbols in gray represent data from the Harvard-Smithsonian molecular database (Ref. 34).

levels higher in energy. As J increases, $b'(v=7)$ approaches from above more closely and its contribution dominates, with the e levels now much lower in energy.

Also shown in Fig. 2 is the indicative rotational structure of the $C^3\Pi_u(v=17)$ valence level that is responsible for the local-intensity perturbation of $c(v=2)$, computed using the CSE model. As can be seen from the figure, $C^3\Pi_u(v=17)$ crosses $c^1\Pi_u(v=2)$ at significantly different J values for each isotopomer. The model crossing points agree with the observed positions of maximum intensity perturbation for both $^{15}N_2$ and $^{14}N^{15}N$. However, for $^{14}N_2$, the $C^3\Pi_u(v=17)$ state is predicted to cross $c^1\Pi_u(v=2)$ at $J \approx 23$, too high to be accessible with the current experimental setup.

One of the main aims of the present work is to examine the character of the local perturbation of $c(v=2)$ by $C(v=17)$. In order to facilitate this in the case of the e -parity levels, we attempt to first remove the effects of the stronger perturbation by $b'(v=7)$ by performing a two-level deperturbation analysis. In the case of the f -parity levels, this procedure is not necessary, the avoided crossing between $b(v=11)$ and $c(v=2)$ occurring only at high- J levels, beyond the range of interest for the $C(v=17)$ crossing.

Effective two-level-deperturbed spectroscopic parameters have been determined from the experimental transition energies for the $c-X(2,0)$ and $b'-X(7,0)$ bands, using a nonlinear least-squares fitting procedure, and omitting the $J=5-13$ and $J=17-18$ $c(v=2)$ -state levels, for $^{15}N_2$ and $^{14}N^{15}N$, respectively, that correspond to the regions of observed intensity perturbation. For $^{14}N_2$, no unusual intensity behavior is observed, so all levels have been included in the analysis. The terms of the ground state $X^1\Sigma_g^+$ are represented by

$$F(J'') = B[J''(J'' + 1)] - D[J''(J'' + 1)]^2 + H[J''(J'' + 1)]^3, \quad (3)$$

where J'' labels the rotational levels of the ground state, B is the rotational constant, and D and H are centrifugal distortion parameters. The spectroscopic parameters of Bendtsen³⁵ and Trickl *et al.*³⁶ are used for the $X^1\Sigma_g^+$ states of $^{15}N_2$, $^{14}N^{15}N$, and $^{14}N_2$. The terms for the excited $c^1\Pi_u$ state, where, for simplicity, we denote the rotational quantum number by J , rather than J' (and the same holds for v and v'), are taken to have the following form:

$$T_f(J) = \nu_0 + B[J(J + 1) - 1] - D[J(J + 1) - 1]^2, \quad (4)$$

for the f -parity²⁴ levels, where ν_0 is the band origin, and

$$T_e(J) = T_f(J) + q[J(J + 1) - 1], \quad (5)$$

for the e -parity levels, where q is the Λ -doubling parameter.

The terms for $b'(v=7)$, which has only e -parity levels, are represented by

$$T(J) = \nu_0 + B[J(J + 1)] - D[J(J + 1)]^2. \quad (6)$$

As already noted, the interaction between the $b'(v=7)$ levels, of $^1\Sigma_u^+$ symmetry, and $c(v=2)$ levels, of $^1\Pi_u$ symmetry, is of a heterogeneous nature ($\Delta\Omega=1$, L-uncoupling) and only involves the e -parity levels of the $c(v=2)$ state. For the e -parity manifold, a two-state deperturbation analysis was

TABLE VII. Two-level-deperturbed molecular parameters for the $c^1\Pi_u(v=2)$ and $b'^1\Sigma_u^+(v=7)$ levels of $^{14}N_2$, $^{14}N^{15}N$, and $^{15}N_2$. All values are in cm^{-1} . Statistical uncertainties (1σ), resulting from the fit, are shown in parentheses, in units of the last significant figure. Additional systematic uncertainties of order 0.05 cm^{-1} apply to the band origins ν_0 .

Species	$^{14}N_2$	$^{14}N^{15}N$	$^{15}N_2$
$c^1\Pi_u(v=2)$			
B	1.821(1)	1.764(1)	1.720(3)
$D \times 10^6$	60(4)	74(5)	151(9)
$q \times 10^3$	38(2)	38(2)	17(3)
ν_0	108 696.32(5)	108 626.57(4)	108 556.38(5)
$b'^1\Sigma_u^+(v=7)$			
B	1.327(2)	1.278(1)	1.243(2)
$D \times 10^6$	-110(7)	-64(6)	-11(9)
ν_0	108 952.02(5)	108 877.89(5)	108 801.35(7)
$H_{b'(7)c(2)}$	2.84(4)	2.76(5)	2.07(8)

performed for each J value by diagonalizing the matrix

$$\begin{pmatrix} T_{b'(7)} & H_{b'(7)c(2)}\sqrt{J(J+1)} \\ H_{b'(7)c(2)}\sqrt{J(J+1)} & T_{c(2)} \end{pmatrix}, \quad (7)$$

where the diagonal elements are the term energies of $b'(v=7)$ and $c(v=2)$, given by Eqs. (6) and (5), respectively. The off-diagonal elements represent the effective heterogeneous interaction between the $c(v=2)$ e -parity and $b'(v=7)$ levels. In the weighted fitting procedure, the nominal uncertainty in the absolute transition energy for fully resolved lines of reasonable strength was taken to be 0.1 cm^{-1} . In the case of weak or blended lines, the uncertainty was set to an estimated value in the range of $0.15\text{--}0.30\text{ cm}^{-1}$. For all three isotopomers, the quality of the obtained fit was reasonable. The results of the two-level deperturbation analysis for the three isotopomers are given in Table VII.

It should be noted that the two-level deperturbation performed here is only an approximation, and that, consequently, the spectroscopic parameters in Table VII have limited physical significance. For example, from molecular-orbital configurational arguments, and experimentation with the CSE model, the direct heterogeneous electronic coupling between the $b'^1\Sigma_u^+$ and $c^1\Pi_u$ states is likely to be very small, so it is principally the indirect mechanism involving both the homogeneous $b' \sim c'$ and the heterogeneous $c' \sim c$ electronic couplings that is responsible for the complexity of the observed $c(v=2)$ -level Λ -doubling in Fig. 3 and the anomalous D values for $b'(v=7)$ in Table VII. Consequently, for large J , the effective deperturbation parameter $H_{b'(7)c(2)}$ will not be well represented as J -independent if $c'(v=2)$ is not also explicitly deperturbed concurrently. However, additional possible perturbation partners could not be followed up to sufficiently high J , and an attempted three state analysis [$b(v=11)$, $b'(v=7)$, and $c(v=2)$] gave inconclusive results, as did the further inclusion of $c'(v=2)$. Thus, only the two-state analysis is presented and the higher- J levels for which the model does not apply are left out of the fit. This limitation does not affect our main aim of studying the additional local perturbation of $c(v=2)$ by $C(v=17)$.

B. P/R intensity anomalies in the $b'-X(7,0)$ band

The effective heterogeneous interaction between $c(v=2)$ and $b'(v=7)$ not only produces energy shifts, but also affects the intensities of transitions accessing the corresponding e -parity levels. In particular, the $b'-X(7,0)$ ionization spectra for each isotopomer display significant P/R -branch intensity anomalies, behavior characteristic of transitions into states of mixed Σ and Π character, where each component of the transition is dipole-allowed.

P/R anomalies and their causative quantum-interference mechanism have been described in detail by Lefebvre-Brion and Field.²⁴ Briefly, in the case of a transition from a $^1\Sigma$ initial state to a nominal $^1\Sigma$ level which is perturbed by a lower-lying $^1\Pi$ level, thus corresponding to the present situation, the J dependence of the perturbed R -branch intensity is given by

$$I_R(J''=J-1) \propto Jc_J^2\mu_{\parallel}^2 + (J+1)(1-c_J^2)\mu_{\perp}^2 \pm 2c_J\sqrt{J(J+1)}(1-c_J^2)\mu_{\parallel}\mu_{\perp}, \quad (8)$$

while the P -branch dependence is given by

$$I_P(J''=J+1) \propto (J+1)c_J^2\mu_{\parallel}^2 + J(1-c_J^2)\mu_{\perp}^2 \mp 2c_J\sqrt{J(J+1)}(1-c_J^2)\mu_{\parallel}\mu_{\perp}, \quad (9)$$

where μ_{\parallel} and μ_{\perp} are the unperturbed $^1\Sigma-^1\Sigma$ and $^1\Pi-^1\Sigma$ vibronic transition moments, respectively, and $c_J \geq 0$ is the J -dependent mixing coefficient corresponding to the amount of $^1\Sigma$ character in the perturbed $^1\Sigma$ wave function. In Eqs. (8) and (9), the upper signs apply when the $\Sigma \sim \Pi$ vibronic interaction matrix element $H_{\Sigma\Pi} > 0$, the lower when $H_{\Sigma\Pi} < 0$. The sense of the quantum-interference effect, corresponding to the overall signs of the cross terms in Eqs. (8) and (9), depends on the sign of the product $\mu_{\parallel}\mu_{\perp}H_{\Sigma\Pi}$. In the present case, where the P -branch of the $b'-X(7,0)$ transition is observed to decrease in intensity as a result of the interference effect, evidently, $\mu_{b'X(7,0)}\mu_{cX(2,0)}H_{b'(7)c(2)} > 0$. Note that, as this is an excited-state interaction, we have chosen to express the intensity of the R and P branches in terms of the excited state rotational quantum number J .

To study this phenomenon experimentally, it is necessary to extract information on the intensity of the transitions measured in the ionization spectra. Generally, it is risky to rely on intensities in a $1\text{ XUV}+1'$ UV experiment. However, if one assumes that the ionization cross section and XUV intensity are constant during the measurement, some semi-quantitative information can be extracted from the experimental results.

Relative rotational intensities in well-behaved, unperturbed vibronic transitions of N_2 are given by

$$I \propto g_{J''}^i S_{JJ''}(2J''+1)e^{-B''[J''(J''+1)]/kT}, \quad (10)$$

where $g_{J''}^i$ is the nuclear spin-statistics factor responsible for the well-known rotational-intensity alternation in the homonuclear isotopomers, $S_{JJ''}$ is the Hönl-London factor, B'' is the rotational constant of the ground state, k is the Boltzmann constant, and T is the absolute rotational temperature. In deriving Eq. (10), it is assumed that the ground state has a Boltzmann population distribution. From Eq. (10), by plot-

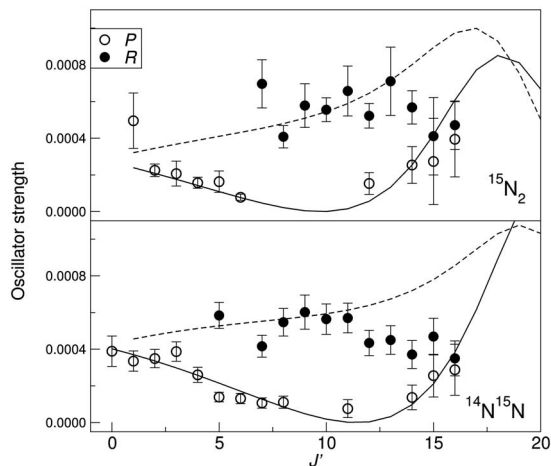


FIG. 4. P/R -branch intensity anomalies in the $b' \ ^1\Sigma_u^+ - X \ ^1\Sigma_g^+(7,0)$ bands of $^{15}\text{N}_2$ and $^{14}\text{N}^{15}\text{N}$. Solid circles: Reduced R -branch intensities (from experimental ionization spectra, see text). Open circles: Reduced P -branch intensities. Solid curve: P -branch band oscillator strengths from CSE-model calculations. Dashed curve: R -branch band oscillator strengths. The experimental reduced intensities have been normalized to the CSE results.

ting $-\ln[I/(g_{J''}^i S_{J''}) (2J''+1)]$ against $J''(J''+1)$, the molecular-beam temperature may be determined from the slope of $B''/(kT)$.

In many cases, Eq. (10) will not apply and the measured ionization signal will be influenced additionally, not only by genuine intensity interference effects, e.g., the P/R anomaly discussed above, but also by J -dependent competition between predissociation and ionization. In order to study these effects, it is instructive to consider the “reduced intensity,” i.e., the actual intensity divided by that implied by Eq. (10), where it is assumed that there is an independent estimate of the molecular-beam temperature(s) available, e.g., from a separate scan over a well-behaved band, taken under similar experimental conditions. The reduced intensity thus serves to highlight any *strongly* J -dependent interference or predissociation effects, with subsequent analysis required to decide between these two possibilities.

In Fig. 4, the reduced intensities (circles) obtained with our 1 XUV+1' UV setup for the P and R branches of the $b' - X(7,0)$ bands in $^{15}\text{N}_2$ and $^{14}\text{N}^{15}\text{N}$ are shown as a function of J , normalized against the corresponding absorption oscillator strengths predicted by our CSE model (curves). The molecular-beam temperature used to determine the reduced intensities was obtained from $c - X(2,0)$ Q -branch lines, measured under virtually the same conditions. For both isotopomers, Fig. 4 shows a remarkable difference in the behavior of the P - and R -branch reduced intensities, with the P -branch intensities exhibiting deep minima at intermediate J values, in good agreement with the CSE-model oscillator strengths. This is a classic example of a P/R intensity anomaly due to the quantum-interference effect described by Eqs. (8) and (9). However, we note that attempts to fit the experimental results in detail using these equations were of limited success, due to the inherently multilevel nature of the N_2 spectrum in this region, which is embodied in the CSE results.

In Fig. 5, the reduced intensities (circles) obtained with

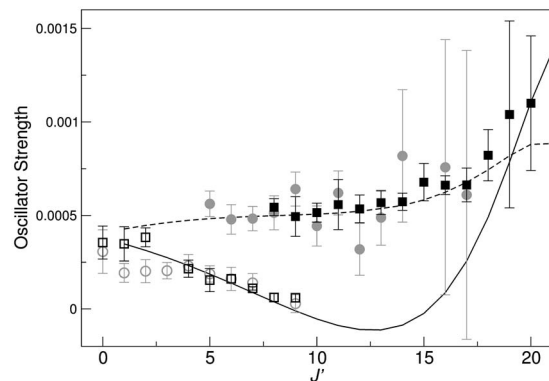


FIG. 5. P/R -branch intensity anomalies in the $b' \ ^1\Sigma_u^+ - X \ ^1\Sigma_g^+(7,0)$ band of $^{14}\text{N}_2$. Solid circles: Reduced R -branch intensities (from experimental ionization spectra, see text). Open circles: Reduced P -branch intensities. Solid curve: P -branch band oscillator strengths from CSE-model calculations. Dashed curve: R -branch band oscillator strengths from CSE-model calculations. Solid squares: R -branch band oscillator strengths from synchrotron-based experiments. Open squares: P -branch band oscillator strengths from synchrotron-based experiments. The experimental reduced intensities have been normalized to the CSE results.

our 1 XUV+1' UV setup in the case of $^{14}\text{N}_2$ are shown, normalized against CSE-model calculations (curves), and compared with absolute band oscillator strengths obtained from our synchrotron-based experiments.³⁷ As for the other isotopomers, once again there is a strong P/R intensity anomaly. It is also of note that the excellent relative agreement between the reduced ionization intensities and the absolute optical oscillator strengths implies that J -dependent predissociation effects are not a factor for $b'(v=7)$, at least for $J \leq 15$.

The quantum-interference effect also influences the e -levels of $c(v=2)$. A pair of equations complementary to Eqs. (8) and (9) can be written to describe the R - and P -branch intensities in the transition to the lower-lying $^1\Pi$ level. In the present case, the R branch of the $c - X(2,0)$ band will suffer the intensity decrease and the P -branch intensity will be enhanced by the interference effect. However, this phenomenon is barely visible in our reduced intensities, since it is both masked by the strong intensity perturbations due to the crossing of $c(v=2)$ by $C(v=17)$, discussed in Sec. IV C, and less prominent due to the much greater oscillator strength of the $c - X(2,0)$ transition.

C. The $c \ ^1\Pi_u(v=2) \sim C \ ^3\Pi_u(v=17)$ interaction

Transitions from the $X \ ^1\Sigma_g^+$ ground state to the $^3\Pi_u$ manifold of N_2 are forbidden by the $\Delta S=0$ selection rule. However, as mentioned in Sec. I, the $^3\Pi_u$ states may spin-orbit couple to the $^1\Pi_u$ states. As a result, transitions to the $^3\Pi_u$ states may become directly observable through their intensity borrowing from dipole-allowed transitions, and/or the $^3\Pi_u$ states may make their presence felt through energy-, intensity-, or line-width-perturbation of the $^1\Pi_u$ states. In the present case, based on CSE-model predictions, we propose that it is the $C \ ^3\Pi_u(v=17)$ level which is responsible for the energy perturbations observed here in the $c(v=2)$ levels of $^{15}\text{N}_2$ and $^{14}\text{N}^{15}\text{N}$. Furthermore, since the $C \ ^3\Pi_u$ state couples electrostatically to the dissociative $C' \ ^3\Pi_u$ state, leading to

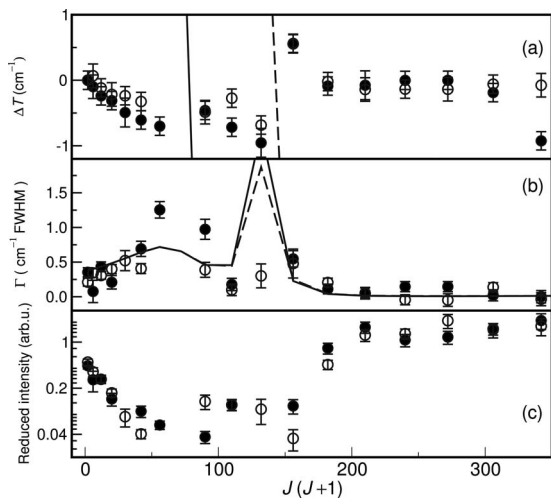


FIG. 6. (a) Reduced terms ΔT for the $c^1\Pi_u(v=2)$ level of $^{15}N_2$. Solid circles: f -parity levels. Open circles: e -parity levels. Solid line: CSE prediction for crossing by $\Omega=1$ sublevel of $C^3\Pi_u(v=17)$. Dashed line: CSE prediction for crossing by $\Omega=0$ sublevel. (b) Predissociation widths for $c^1\Pi_u(v=2)$ in $^{15}N_2$. Solid circles: f -parity levels, from fitting Q -branch line profiles in $c-X(2,0)$ ionization spectra. Open circles: e -parity levels, weighted average of fits to P - and R -branch line profiles. Solid line: CSE-model widths for f levels. Dashed line: CSE-model widths for e levels. (c) Reduced intensities (see text), taking into account the high- (202 K) and low- (25 K) temperature components of the molecular beam. Solid circles: f -parity levels, from integrated Q -branch intensities in $c-X(2,0)$ ionization spectra. Open circles: e -parity levels, weighted average of P - and R -branch reduced intensities.

strong predissociation,¹⁴ it is likely that the local perturbation of $c(v=2)$ by $C(v=17)$ is also responsible for the intensity anomalies observed in the corresponding ionization spectra, through accidental predissociation effects. Due to the complexity of the N_2 structure, however, these conclusions are by no means obvious from an examination of the experimental spectra alone. We attempt to justify them below.

After the perturbations in the singlet manifold have been roughly accounted for and removed, as in Sec. IV A, the residual local energy shifts can be examined. In Fig. 6(a), the reduced term values of the $c(v=2)$ rotational levels are shown for $^{15}N_2$. Both e - and f -parity reduced terms exhibit a similar pattern, with local perturbations evident between $J=7$ and 9, and, more clearly, between $J=11$ and 12. In Fig. 6(b), the fitted Lorentzian line-width components (symbols) for isolated rotational transitions in the $c-X(2,0)$ band of the ionization spectrum of $^{15}N_2$ are presented, with only minor differences observed between the line-width patterns for transitions into the e - and f -parity levels of the $c(v=2)$ state. Considerable predissociation of the $c(v=2)$ -state levels is observed in the region of the local perturbations, with level-width maxima near $J=8$ and 12. In the case of blended lines, term values could be extracted from the experimental spectra, but neither line-width nor intensity information could be obtained reliably. Also shown in Fig. 6(b) are the results of our preliminary CSE-model calculations (lines), which are in good overall agreement with the observed predissociation pattern, but with some discrepancy in the region of the higher- J crossing. Finally, in Fig. 6(c), the reduced intensities for transitions to the e - and f -parity levels of $c(v=2)$ in $^{15}N_2$ are shown. For $J > 14$, these reduced intensities are essen-

tially J -independent. However, at lower J , significant intensity depletion is observed, with deep intensity minima near $J=8$ and 12. In the case of the missing $J=8f$ level, for example, the associated $Q(8)$ line was too weak to be observed. As stated in Sec. IV B, there is no clear evidence of P/R intensity anomalies in the $c-X(2,0)$ spectrum, so the dramatic behavior of the reduced intensities in Fig. 6(c) is likely another signature of predissociation. It is notable that the positions of the intensity minima occur for the same values of J where the line widths and term values also show unusual behavior.

The patterns in Fig. 6, containing only two distinct regions of perturbation, are not directly suggestive of perturbation by a triplet level, despite the CSE model indicating that $C^3\Pi_u(v=17)$ is primarily responsible. There are two reasons for this.

First, only $C_{\Omega=1}(v=17)$ can interact by spin-orbit coupling ($\Delta\Omega=0$) directly with $c_{\Omega=1}(v=2)$. However, as the J -dependent S -uncoupling mechanism ($\Delta\Omega=\pm 1$) induces mixing between $C_{\Omega=1}(v=17)$ and both $C_{\Omega=0}(v=17)$ and $C_{\Omega=2}(v=17)$, the latter substates may also interact indirectly with $c(v=2)$. For the limiting case of a slowly rotating molecule, the $\Omega=1$ component of the triplet perturber will strongly spin-orbit couple to the $c(v=2)$ state, while the $\Omega=0, 2$ components will couple only weakly, corresponding to the Hund's case (a) limit. On the other hand, at high J values, the Hund's case (b) limit is approached, where the $\Omega=0, 2$ components interact strongly with $c(v=2)$, but the $\Omega=1$ component is only weakly coupled.³⁹ The local perturbation culminating near $J=8$ coincides with the CSE-predicted crossing by $C_{\Omega=1}(v=17)$, indicated by the solid line in Fig. 6(a), while that at $J=11-12$ is due to the $\Omega=0$ crossing,³⁸ indicated by the dashed line. The $C_{\Omega=2}(v=17)$ sublevel would be expected to cross $c(v=2)$ in the region of $J=5$, but no evidence for a perturbation associated with this crossing is visible in Fig. 6(a). Part of the reason for this relates to the low J value for the crossing, suggesting that the Hund's case (a) limit will be approached, therefore implying only a weak indirect coupling between $C_{\Omega=2}(v=17)$ and $c_{\Omega=1}(v=2)$. This phenomenon was also observed in the $k^3\Pi$ state of CO, which is spin-orbit coupled to the $E^1\Pi$ state, causing predissociation in the same manner as in the present study (see Fig. 12 of Ref. 40).

Second, the characteristics of local perturbations in energy depend also on the predissociation width of the perturbing level. For example, perturbation by a long-lived level results in a perturbation with a rapid J -dependence and a maximum shift at the crossing, while perturbation by a short-lived level may result in a barely noticeable perturbation with a slow J -dependence and *zero* shift at the crossing. In the case of crossing by a triplet level, the visibility and character of the associated perturbations will also depend on the relative predissociation widths of the triplet sublevels. In the present case, the CSE model predicts that the lowest $C(v=17)$ sublevel ($\Omega=2$) is very strongly predissociated, with the level widths, also strongly J -dependent, decreasing significantly for $\Omega=1$, and $\Omega=0$, respectively. Thus, primarily due to the large width of $C_{\Omega=2}(v=17)$ relative to the spin-splitting of the triplet state, only the highest two of the ex-

pected three energy perturbations in the $c(v=2)$ level are visible in Fig. 6(a).

For the same reasons, only two clear peaks are visible in the $c(v=2)$ predissociation pattern in Fig. 6(b), and two minima in the associated intensity-depletion pattern in Fig. 6(c). In particular, the higher- J crossing, corresponding to the better defined local perturbation in Fig. 6(a), is seen in Fig. 6(b) to be associated with the most rapid variation in the computed predissociation line width which is borrowed by $c(v=2)$ from the $C(v=17)$ perturber. It is notable that, while the energy perturbations in the $c(v=2)$ level of $^{15}\text{N}_2$ caused by the crossing with the short-lived $C(v=17)$ level are small, the corresponding indirect predissociations and intensity depletions are dramatic, despite the weak spin-orbit coupling, because of the otherwise long inherent lifetime of $c(v=2)$.

Finally, we emphasize that caution is necessary when trying to infer detailed information on the perturbing $C(v=17)$ level from the experimental spectra, with simplistic level deperturbations of little use. Detailed examination of the CSE model indicates that the $^3\Pi_u$ manifold in this energy region is of great complexity, with the $F^3\Pi_u$ and $G^3\Pi_u$ Rydberg states also having an active influence on the character of the $c(v=2) \sim C(v=17)$ perturbation. In fact, the very strongly predissociated $F(v=2)$ level, which also contains a significant G -state admixture,²¹ crosses $C(v=17)$ in the region of the latter level's crossing with $c(v=2)$, for all isotopomers, leading, e.g., to the irregularities in the computed nominal $C(v=17)$ -level energies for $^{14}\text{N}_2$ displayed in Fig. 2. In addition, electrostatic interactions within the $^3\Pi_u$ manifold lead to strong J - and Ω -dependences in the $C(v=17)$ predissociation line widths, as mentioned above, which further complicate interpretation of the data. In particular, the determination of $C(v=17)$ sublevel rotational terms becomes impossible when the corresponding predissociation line widths are comparable to, or larger than, the spin splitting.

The results for $^{14}\text{N}^{15}\text{N}$ (summarized in Fig. 7) are more equivocal. For this isotopomer, the crossing of $c(v=2)$ by $C(v=17)$ is predicted by the CSE model to occur in the region of $J=17$. In Fig. 7(a), no significant term-value shifts can be observed for the f -parity levels, but there is evidence of a weak local perturbation between $J=17$ and 18 in the e -parity levels. Overall, the fitted Lorentzian line widths in Fig. 7(b) (symbols) are not conclusive, because of large error bars in the crossing region, but are not inconsistent with the computed CSE-model widths (lines), which predict a predissociation maximum in the $J=17$ –18 region. The reduced intensities in Fig. 7(c), however, show fairly clear depletion, displaying a single minimum near $J=18$, which is shaded towards lower J -values, behavior consistent with that expected from the computed line widths. Taken together, the experimental results are consistent with the perturbation of $c(v=2)$ by $C(v=17)$ in the $J=17$ –18 region, but imply such a strong predissociation of the $C(v=17)$ sublevels that (1) the associated energy shifts are only small, and (2) the predissociation signatures collapse into a single broad feature. This is supported by the CSE results, which suggest that it is the $\Omega=0$ sublevel of $C(v=17)$, indicated by the dashed line in Fig. 7(a), that has the lowest predissociation width and is

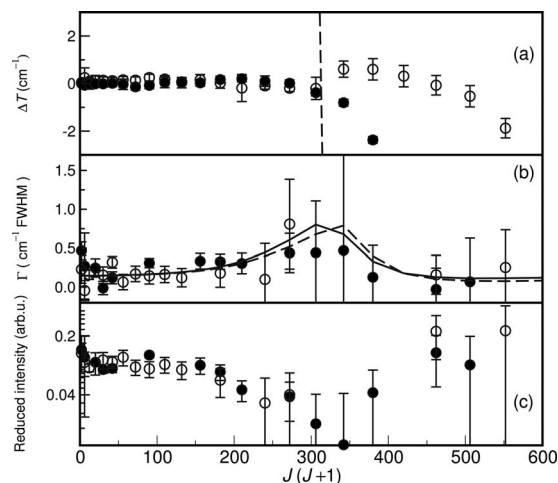


FIG. 7. (a) Reduced terms ΔT for the $c^1\Pi_u(v=2)$ level of $^{14}\text{N}^{15}\text{N}$. Solid circles: f -parity levels. Open circles: e -parity levels. Dashed line: CSE prediction for crossing by $\Omega=0$ sublevel. (b) Predissociation widths for $c^1\Pi_u(v=2)$ in $^{14}\text{N}^{15}\text{N}$. Solid circles: f -parity levels, from fitting Q -branch line profiles in $c-X(2,0)$ ionization spectra. Open circles: e -parity levels, weighted average of fits to P - and R -branch line profiles. Solid line: CSE-model widths for f levels. Dashed line: CSE-model widths for e levels. (c) Reduced intensities (see text), taking into account the high- (275 K) and low- (72 K) temperature components of the molecular beam: Solid circles: f -parity levels, from integrated Q -branch intensities in $c-X(2,0)$ ionization spectra. Open circles: e -parity levels, weighted average of P - and R -branch reduced intensities.

responsible for the only local perturbation evident in the $c(v=2)$ terms, with the other sublevels so broad that no corresponding shifts occur.

As stated in Sec. IV A, for $^{14}\text{N}_2$, the CSE model predicts the crossing between $c(v=2)$ and $C(v=17)$ to take place in the region of $J=23$ (see Fig. 2). Since, under our experimental conditions, such high-rotational levels cannot be accessed with the laser-based system, the fact that no energy-level shifts or intensity anomalies have been observed in the present data for this isotopomer is hardly surprising. Nevertheless (in Fig. 8), we are able to compare the synchrotron-based predissociation widths for the $c(v=2)$ level of $^{14}\text{N}_2$ (circles)³⁷ with the CSE-model values (lines). The CSE results indicate a marginally double-peaked structure, with pre-

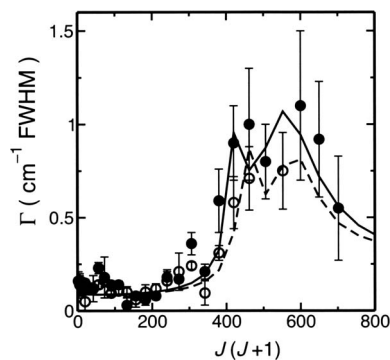


FIG. 8. Comparison between experimental predissociation line widths for the $c^1\Pi_u(v=2)$ level of $^{14}\text{N}_2$, derived from synchrotron-based photoabsorption spectroscopy of the $c-X(2,0)$ band (Ref. 29), and CSE-model calculations. Solid circles: Experimental values from fits to Q -branch transitions. Open circles: Weighted average of experimental values from P - and R -branch transitions. Solid line: CSE widths for f -parity levels. Dashed line: CSE widths for e -parity levels.

dissociation maxima near $J=20-21$ and $23-24$, in excellent agreement with the measurements. Once again, the short lifetime of the $C(v=17)$ perturber, together with the complex interactions at play, combine to severely modify the expected triplet pattern of predissociation. For this isotopomer, it is the $\Omega=2$ sublevel of $C(v=17)$ which has the lowest predissociation width and is responsible for the first $c(v=2)$ predissociation maximum in Fig. 8, while the broader $\Omega=1,0$ sublevels contribute to the second maximum, with the $\Omega=1$ contribution likely to be smaller because of the case-(b) nature of this high- J crossing.

V. SUMMARY AND CONCLUSIONS

The $3p\pi_u c^1\Pi_u - X^1\Sigma_g^+(2,0)$ Rydberg and $b'^1\Sigma_u^+ - X^1\Sigma_g^+(7,0)$ valence transitions of $^{14}N_2$, $^{14}N^{15}N$, and $^{15}N_2$ have been studied using laser-based $1\text{ XUV}+1'\text{ UV}$ two-photon-ionization spectroscopy, supplemented by synchrotron-based XUV spectroscopy in the case of $^{14}N_2$. Due to the inherent complexity and multilevel nature of the N_2 structure and spectrum in this energy region, few-level deperturbation techniques were found to be of limited use and interpretation of the results by means of coupled-channel Schrödinger-equation techniques was found necessary.

For each isotopomer, effective rotational interactions between the $c(v=2)$ and $b'(v=7)$ levels were found to cause strong Λ -doubling in $c(v=2)$, together with dramatic P/R -branch intensity anomalies in the $b'-X(7,0)$ band due to the effects of quantum interference. The P/R intensity anomalies for all isotopomers, together with the synchrotron-based oscillator strengths for $^{14}N_2$, were found to be well described by the present CSE calculations.

Local perturbations in energy and predissociation line width for the $c(v=2)$ Rydberg level were observed and attributed primarily to a spin-orbit interaction with the crossing, short-lived $C^3\Pi_u(v=17)$ valence level. However, the CSE calculations suggest that this is a complex interaction, also involving the even shorter-lived $F(v=2)$ Rydberg level in the same energy region. The characterization of these interactions should further help to elucidate the predissociation mechanism for the $^1\Pi_u$ states of N_2 ,¹⁴ extending the applicability of the corresponding CSE code towards higher energies.

ACKNOWLEDGMENTS

This research was partially supported by Australian Research Council Discovery Program Grant Nos. DP0558962 and DP0773050.

- ¹D. Stahel, M. Leoni, and K. Dressler, *J. Chem. Phys.* **79**, 2541 (1983).
- ²D. Spelsberg and W. Meyer, *J. Chem. Phys.* **115**, 6438 (2001).
- ³S. A. Edwards, W.-Ü. L. Tchang-Brillet, J.-Y. Roncin, F. Launay, and F. Rostas, *Planet. Space Sci.* **43**, 67 (1995).
- ⁴M. O. Vieitez, T. I. Ivanov, J. P. Sprengers, C. A. de Lange, W. Ubachs, B. R. Lewis, and G. Stark, *Mol. Phys.* **105**, 1543 (2007).
- ⁵P. K. Carroll and C. P. Collins, *Can. J. Phys.* **47**, 563 (1969).

- ⁶G. Stark, K. P. Huber, K. Yoshino, P. L. Smith, and K. Ito, *J. Chem. Phys.* **123**, 214303 (2005).
- ⁷W. Ubachs, L. Tashiro, and R. N. Zare, *Chem. Phys.* **130**, 1 (1989).
- ⁸W. Ubachs, I. Velchev, and A. de Lange, *J. Chem. Phys.* **112**, 5711 (2000).
- ⁹W. Ubachs, R. Lang, I. Velchev, W.-Ü. L. Tchang-Brillet, A. Johansson, Z. S. Li, V. Likhnygin, and C.-G. Wahlström, *Chem. Phys.* **270**, 215 (2001).
- ¹⁰C. W. Walter, P. C. Cosby, and H. Helm, *J. Chem. Phys.* **99**, 3553 (1993).
- ¹¹A. B. van der Kamp, P. C. Cosby, and W. J. van der Zande, *Chem. Phys.* **184**, 319 (1994).
- ¹²J. P. Sprengers, W. Ubachs, K. G. H. Baldwin, B. R. Lewis, and W.-Ü. L. Tchang-Brillet, *J. Chem. Phys.* **119**, 3160 (2003).
- ¹³M. Leoni and K. Dressler, *ZAMP* **22**, 794 (1971).
- ¹⁴B. R. Lewis, S. T. Gibson, W. Zhang, H. Lefebvre-Brion, and J.-M. Robbe, *J. Chem. Phys.* **122**, 144302 (2005).
- ¹⁵P. K. Carroll and R. S. Mulliken, *J. Chem. Phys.* **43**, 2170 (1965).
- ¹⁶V. E. Haverd, B. R. Lewis, S. T. Gibson, and G. Stark, *J. Chem. Phys.* **123**, 214304 (2005).
- ¹⁷J. P. Sprengers, W. Ubachs, A. Johansson, A. L'Huillier, C.-G. Wahlström, B. R. Lewis, and S. T. Gibson, *J. Chem. Phys.* **120**, 8973 (2004).
- ¹⁸B. R. Lewis, S. T. Gibson, J. P. Sprengers, W. Ubachs, A. Johansson, and C.-G. Wahlström, *J. Chem. Phys.* **123**, 236101 (2005).
- ¹⁹J. P. Sprengers, E. Reinhold, W. Ubachs, K. G. H. Baldwin, and B. R. Lewis, *J. Chem. Phys.* **123**, 144315 (2005).
- ²⁰T. Hashimoto and H. Kanamori, *Chem. Phys. Lett.* **235**, 104 (2006).
- ²¹B. R. Lewis, A. N. Heays, S. T. Gibson, H. Lefebvre-Brion, and R. Lefebvre, "A coupled-channel model of the $^3\Pi_u$ states of N_2 : Structure and interactions of the $F^3\Pi_u$ and $G^3\Pi_u$ Rydberg states," *J. Chem. Phys.* (to be published).
- ²²J. P. Sprengers, Ph.D. thesis, Vrije Universiteit, Amsterdam, 2006.
- ²³B. R. Lewis, K. G. H. Baldwin, J. P. Sprengers, W. Ubachs, G. Stark, and K. Yoshino, "Optical observation of the C , F , and $G^3\Pi_u$ states of N_2 ," *J. Chem. Phys.* (to be published).
- ²⁴H. Lefebvre-Brion and R. W. Field, *The Spectra and Dynamics of Diatomic Molecules* (Elsevier, Amsterdam, 2004), pp. 144, 378–386, 400, and 540.
- ²⁵W. Ubachs, K. S. E. Eikema, and W. Hogervorst, *Appl. Phys. B: Lasers Opt.* **57**, 411 (1993).
- ²⁶S. Gerstenkorn and P. Luc, "Atlas du spectra d'absorption de la molecule d'iode," Laboratoire Aimé Cotton, CNRS II, 91405 Orsay (France), 15 600–17 600 cm^{-1} (1977).
- ²⁷K. S. E. Eikema, W. Hogervorst, and W. Ubachs, *Chem. Phys.* **181**, 217 (1994).
- ²⁸S. N. Dobryakov and Y. S. Lebedev, *Sov. Phys. Dokl.* **13**, 873 (1969).
- ²⁹G. Stark, B. R. Lewis, A. N. Heays, K. Yoshino, P. L. Smith, and K. Ito, *J. Chem. Phys.* **128**, 114302 (2008).
- ³⁰X. Liu, D. E. Shemansky, C. P. Malone, P. V. Johnson, J. M. Ajello, I. Kanik, A. N. Heays, B. R. Lewis, S. T. Gibson, and G. Stark, *J. Geophys. Res.* **113**, A02304 (2008).
- ³¹M.-C. Liang, A. N. Heays, B. R. Lewis, S. T. Gibson, and Y. L. Yung, *Astrophys. J.* **664**, L115 (2007).
- ³²E. F. van Dishoeck, M. C. van Hemert, A. C. Allison, and A. Dalgarno, *J. Chem. Phys.* **81**, 5709 (1984).
- ³³B. R. Lewis, S. T. Gibson, F. T. Hawes, and L. W. Torop, *Phys. Chem. Earth, Part C, Sol. Terr. Planet. Sci.* **26**, 519 (2001).
- ³⁴www.cfa.harvard.edu/amp/ampdata/cfamols.html.
- ³⁵J. Bendtsen, *J. Raman Spectrosc.* **32**, 989 (2001).
- ³⁶T. Trickl, D. Proch, and K. L. Kompa, *J. Mol. Spectrosc.* **171**, 374 (1995).
- ³⁷These synchrotron-based results have also been reported in Ref. 29.
- ³⁸The $C^3\Pi_u$ state is normal for the lower vibrational levels, but *inverted* in this region (Ref. 23).
- ³⁹I. Kovacs, *Rotational Structure in the Spectra of Diatomic Molecules* (Hilger, London, 1969), pp. 272–274.
- ⁴⁰P. Cacciani, W. Hogervorst, and W. Ubachs, *J. Chem. Phys.* **102**, 8308 (1995).